

THE USE OF RADIAL VELOCITY DERIVATIVE TO DIAGNOSE ROTATION AND DIVERGENCE

Travis M. Smith^{1,2,*} and Kimberly L. Elmore^{1,2}¹Cooperative Institute for Mesoscale Meteorology Studies, University Of Oklahoma, Norman, Oklahoma.²NOAA/National Severe Storms Laboratory, Norman, Oklahoma.**1. Introduction**

Traditional methods of calculating rotational and divergent shears from Doppler radial velocity data can give results that vary widely from the true value of shear for the meteorological feature being sampled. Some factors that must be considered include noisy data, the azimuthal offset of sample volumes from the center of the feature (Wood and Brown 1997), and the radar viewing angle. One commonly used technique relies simply on the difference of the maximum and minimum radial velocity within a rotation or divergence feature. This method is plagued with uncertainties in the values of the shear estimates as well in locating the center of a shear feature. This work illustrates results from a two-dimensional, local, linear least squares (LLSD) method to minimize the large variances in rotational and divergent shear calculations.

There are several benefits of using LLSD first derivative (shear) estimates. They are tolerant of the noisy data which are typical of radial velocity data. LLSD data are adaptable to various spatial scales. Two-dimensional LLSD techniques are more noise tolerant than one-dimensional LLSD techniques, but give lower values of shear as a result.

Besides creating greater confidence in the value of intensity of meteorological features that are sampled, the LLSD method for calculating shear values has several other advantages. The LLSD removes many of the radar dependencies involved in the detection of rotation and radial divergence (or radial convergence) signatures. Thus, these derivatives of the radial velocity field may be viewed in three-dimensional space or used as input to multi-sensor meteorological applications that require more than one radar as input. Additionally, fields of these radial estimates of

rotation and divergence have specific signatures when boundaries or circulations are sampled.

This manuscript describes how the derivatives are calculated as well as how the rotational and divergent LLSD compares with the less-robust (but frequently used) “peak-to-peak” estimates of azimuthal shear and radial divergence. We use idealized models to quantify the errors of the LLSD and “peak-to-peak” estimates. Finally, we show examples of how this technique performs on radar data collected during convective events.

2. Method*a. Derivation*

Elmore et al. (1994) describe a method for estimating divergent shear from single Doppler radar data for use in calculating headwind loss estimates for aircraft that encounter microbursts. The rotation portion of the derivative was also derived by Elmore et al. (1994), but not utilized for microburst detection. The LLSD technique was implemented in NSSL’s Damaging Downburst Prediction and Detection Algorithm (Smith et al. 2004) for detecting low-level outflows and mid-level convergence and rotation in storm cells. Mitchell and Elmore (1998) first explored the uses of the LLSD for identifying regions of high shear in mesocyclones and tornadic vortex signatures. We have built upon these earlier works in order to improve the robustness of the LLSD and to evaluate its performance as a tool to interrogate meteorological features detected by Doppler radar. The derivation (Elmore et al. 1994) follows.

If we let $u(r,\theta)$ be the radial velocity at range r and azimuth angle θ , then the most obvious way to estimate the divergent and rotational derivatives is to calculate u_r (the partial derivative of u with respect to r) and u_s (the

partial derivatives of u with respect to θ). The idea is to treat $u(r, \theta)$ as a scalar field since we have no information about the true direction of the wind at a point (r, θ) . We would like to compute (u_x, u_y) (the gradient). This vector gives the direction of the most rapid change in the field, and the magnitude of this vector gives the largest rate of change in any direction at the point. Since the data is not given in Cartesian coordinates, but in polar coordinates from the radar, we introduce some new variables that are easier to use.

At the point (r, θ) , we introduce the variable $s = r\varphi$, where φ is the signed angle measured from the reference line θ , with positive angles measured in the counterclockwise direction. One can show (using the chain rule) that $u_r^2 + u_s^2 = u_x^2 + u_y^2$ at (r, θ) . So the largest rate of change of the field in any direction at (r, θ) is given by:

$$(u_r^2 + u_s^2)^{1/2}.$$

We now give estimates for u_r and u_s . We assume the data are given at regular intervals of Δr and $\Delta\varphi$. This assumption makes our computations fast, since we can give our estimates in closed form.

We fit the data locally by a model of the form:

$$\tilde{u}(r, s) = u_0 + u_r(r - r_0) + u_s s.$$

At the point (r_i, φ_j) , $\Delta r_i = r_i - r_0 = i\Delta r$ and $s_{ij} = r_i\varphi_j = (r_0 + i\Delta r)(j\Delta\varphi)$. Let $\Delta s_{ij} = (s_{ij} - s_0)$ where we have taken $s_0 = r_0\varphi_0 = 0$, since we have $\varphi_0 = 0$. We pick our model by a least squares method, i.e. we pick the constants u_0, u_r, u_s as to minimize the quadratic

$$R = \sum [u(r_i, s_j) - \tilde{u}(r_i, s_{ij})]^2 w_{ij},$$

where w_{ij} is a weight function with $w_{ij} > 0$ and $w_{-i, j} = w_{i, j}$ and $w_{i, -j} = w_{i, j}$ for all i and j . This symmetry assumption allows for a simple closed-form solution for u_0, u_r, u_s . The normal equations are given by

$$\frac{R}{\partial u_r} = \frac{\partial R}{\partial u_s} = \frac{\partial R}{\partial u_0} = 0$$

Expanding the above, we obtain the normal equations:

$$(\sum \Delta r_i^2 w_{ij}) u_r + (\sum \Delta r_i \Delta s_{ij} w_{ij}) u_s + (\sum \Delta r_i w_{ij}) u_0 = \sum \Delta r_i u_{ij} w_{ij},$$

$$(\sum \Delta r_i \Delta s_{ij} w_{ij}) u_r + (\sum \Delta s_{ij}^2 w_{ij}) u_s + (\sum \Delta s_{ij} w_{ij}) u_0 = \sum \Delta s_{ij} u_{ij} w_{ij},$$

$$(\sum \Delta r_i w_{ij}) u_r + (\sum \Delta s_{ij} w_{ij}) u_s + (\sum w_{ij}) u_0 = \sum u_{ij} w_{ij},$$

where Σ is over all i and j , and u_{ij} is the data $u_{ij} = u(r_i, s_{ij})$. We next assume symmetry in the data locations about the point (r_0, s_0) . For example, we assume i runs from $-N, \dots, 0, 1, \dots, N$ and j runs from $-M, \dots, 0, 1, \dots, M$. Using these symmetry assumptions, all off-diagonal coefficients vanish. This leaves a simple diagonal system to solve:

$$u_r = \frac{\sum i u_{ij} w_{ij}}{\Delta r \sum i^2 w_{ij}}$$

$$u_s = \frac{\sum s_{ij} u_{ij} w_{ij}}{\sum (\Delta s_{ij})^2 w_{ij}}$$

$$u_0 = \frac{\sum u_{ij} w_{ij}}{\sum w_{ij}}$$

b. Application

In order to make LLSD calculations on a polar grid of radial velocities, the data are passed through a 3x3 median filter to reduce noise. Then we apply the formulae for u_r and u_s . Because u_r and u_s are derived from only the radial component of the wind, they are approximations of one half the horizontal divergence ("half divergence", hereafter) and vertical vorticity ("half vorticity", hereafter), respectively, assuming a symmetric wind field. This symmetry assumption works well in the vicinity of features that may be purely rotational, such as mesocyclones, or divergent, such as symmetric downburst signatures. Although it breaks down for asymmetric features such as gust fronts, useful information may still be gleaned from the LLSD output in many cases.

Due to the nature of polar grids, the size of the kernel that is used in the LLSD calculations varies in range. We have chosen to use a kernel that maintains a nearly constant width in Cartesian space, meaning that the number of

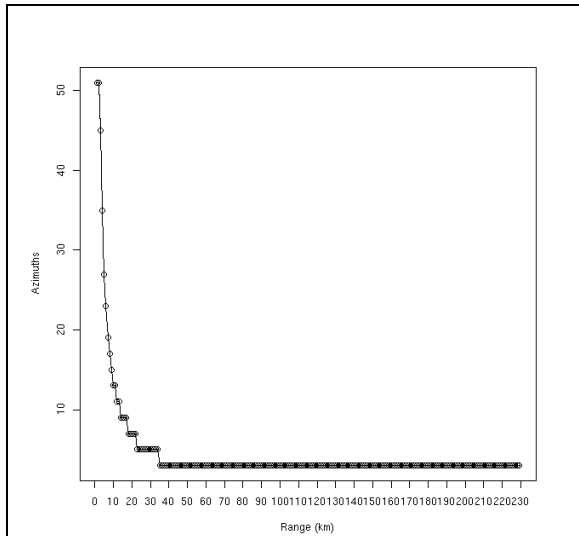


Figure 1: The number of azimuths used for a 2500 m wide kernel by range.

radials used by each radar pixel is a function of range.

3. LLSD Rotational Shear

LLSD rotational, or azimuthal, shears are calculated for simulated circulation signatures of different sizes and at different ranges from a hypothetical radar with 1° azimuthal spacing in order to compare with traditional methods of estimating the strength of circulations. We use a Rankine combined vortex model to generate simulated circulation signatures in the Doppler radial velocity field (Wood and Brown 1997). We superimpose 2 ms^{-1} uniform noise on the radial velocity field to test the robustness of the LLSD calculations.

We compare the LLSD values to the more traditional “peak-to-peak” azimuthal shear calculation, given by

$$u_{as} = \frac{V_{max} - V_{min}}{d}$$

where V_{max} and V_{min} are the maximum outbound and minimum inbound radial velocities (on opposite sides of a circulation), respectively, and d is the distance between those two peaks. For the rotational LLSD calculations, we choose three different kernel sizes that are each 3 range gates deep and approximately 2500 m, 5000 m, or 8000 m wide. Thus the number of radials used in the calculation varies with range from the radar (Fig. 1), although a minimum of three

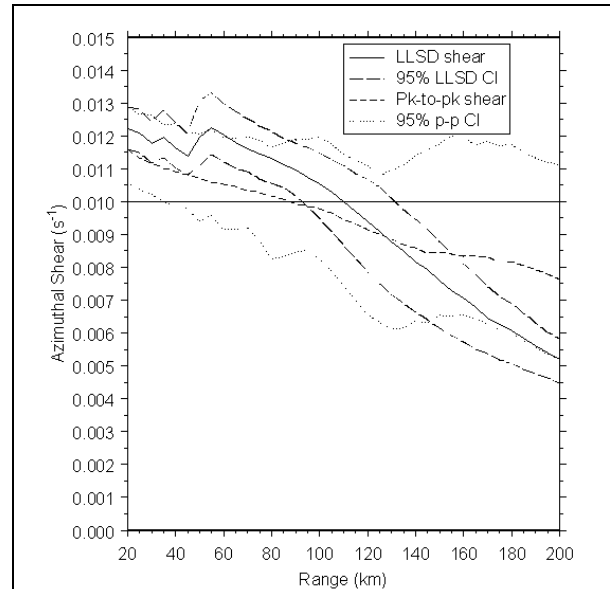


Figure 2: Mean and 95% confidence limits for LLSD and peak-to-peak estimates of azimuthal shear at the vortex center for a 5 km diameter vortex with half vorticity of 0.01 s^{-1} .

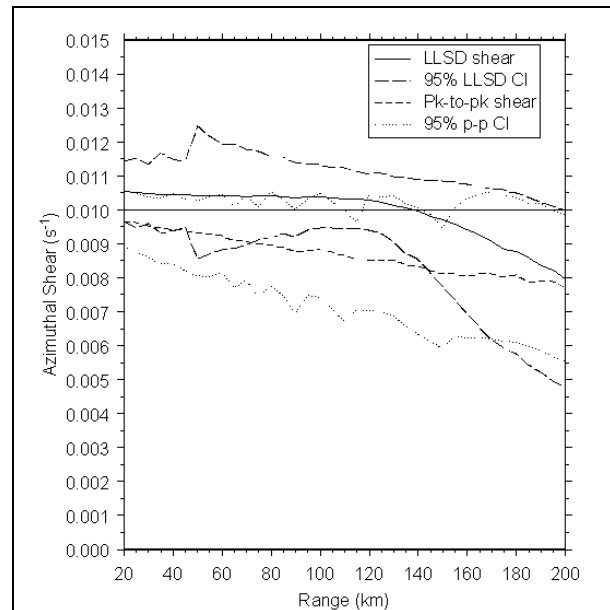


Figure 3: Mean and 95% confidence limits for LLSD and peak-to-peak estimates of azimuthal shear at the vortex center for an 8 km diameter vortex with half vorticity of 0.01 s^{-1} .

radials of data are required for a complete calculation. Kernels that use a fixed number of radials at all ranges usually only provide good shear estimates in a small percentage of those ranges.

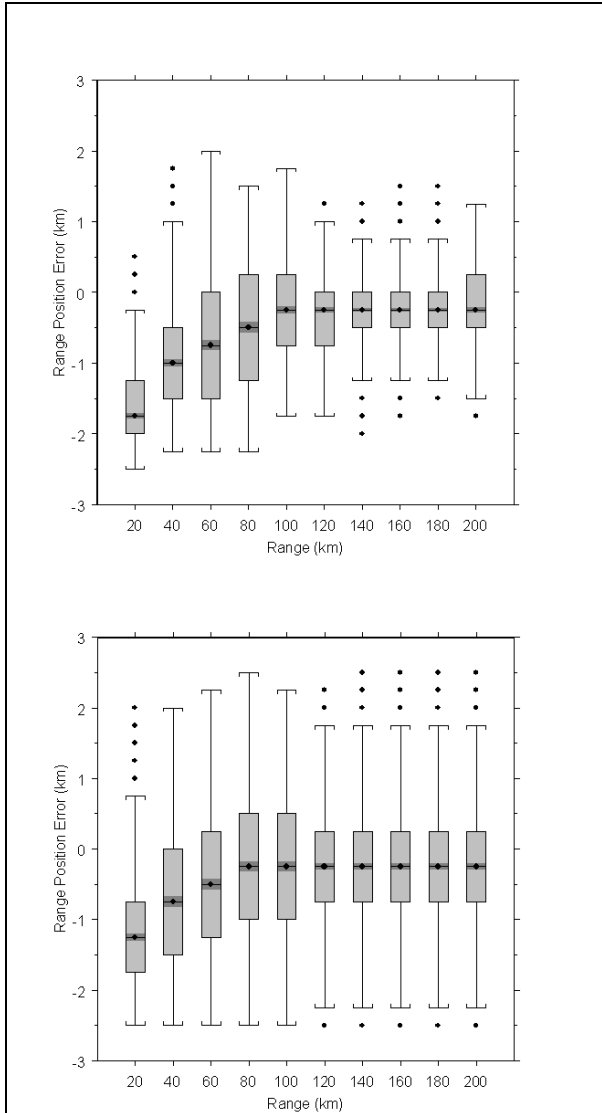


Figure 4: The distribution of range positional errors for the 2500 m LLSD kernel (top) and the peak-to-peak azimuthal shear estimate (bottom) for a 5 km diameter vortex. The center grey line is the median, the box is the interquartile range (IQR), the whiskers are the lesser of 1.5x(IQR) or the data range, and the single dots are outliers.

To test the variability of the three LLSD kernels, we generate synthetic radial velocity signatures of vortices at ranges every 5 km from 20 km to 200 km. Because radar data suffer from many imperfections, including noise and sampling issues that can affect azimuthal shear values (Wood and Brown 2000), 1000 vortices of the same size and strength are generated at each range, each with different noise patterns

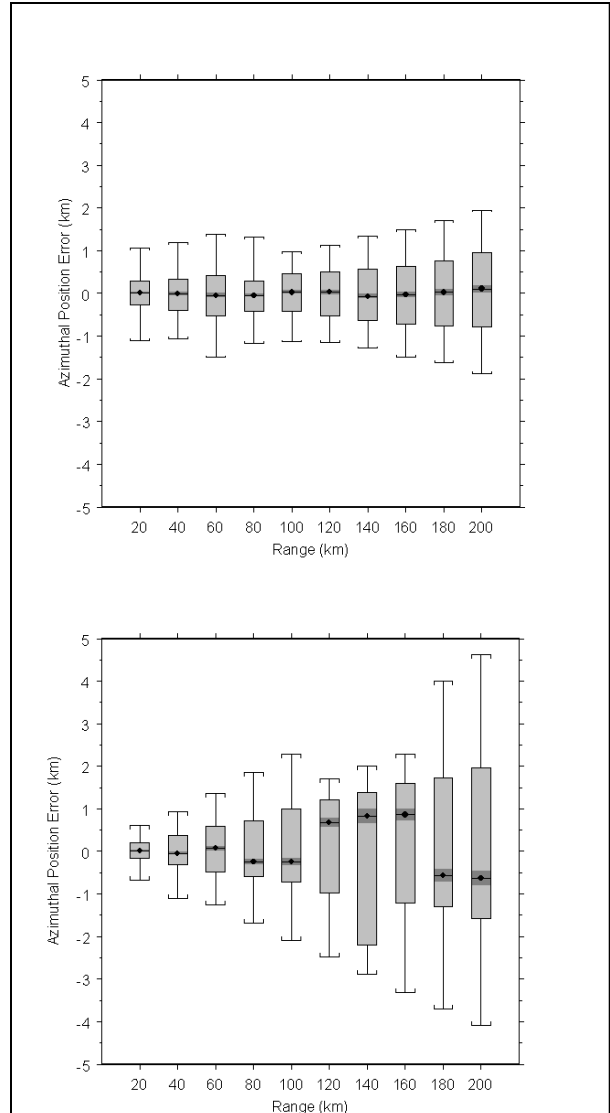


Figure 5: Same as Fig. 3, except for azimuthal position error.

and azimuthal offsets to the center of the simulated vortex. This allows for calculation of mean azimuthal shear values and 95% confidence intervals for the three LLSD kernels and u_{as} .

Figure 2 shows the 2500m LLSD kernel and peak-to-peak azimuthal shear estimates for a 5 km diameter vortex with half vorticity of 0.01 s^{-1} . In this case, the mean LLSD value is within about 20% of the true value out to about 140 km, with a much smaller variance than that of the peak-to-peak azimuthal shear calculations. These values drop with range because of the geometry of the radar beam – circulations are not well sampled at long ranges. For a larger-scale 8 km diameter vortex (Fig. 3) sampled with

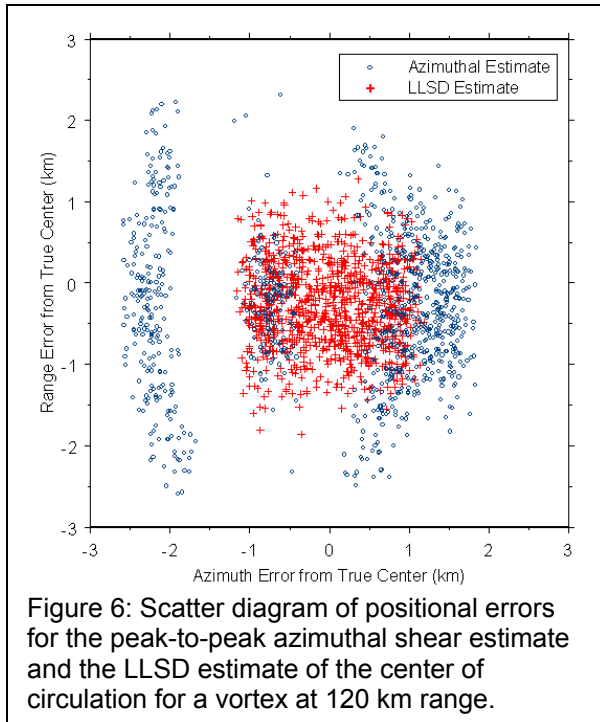


Figure 6: Scatter diagram of positional errors for the peak-to-peak azimuthal shear estimate and the LLSD estimate of the center of circulation for a vortex at 120 km range.

the 2500 m kernel, the mean LLSD values are within 5% of the true value out to about 150 km. For brevity, results from the 5000 m and 8000 m kernel are not shown. However, these larger kernels tended to underestimate the strength of smaller vortices compared to the 2500 m kernel.

Because we use synthetic radar data, the true location of the center of the circulation is known. Range and azimuthal position errors were calculated for both the LLSD and peak-to-peak methods. For azimuthal shear, the center of circulation was considered to be halfway between velocity absolute maxima on each side of the circulation. The NSSL Mesocyclone Detection Algorithm (Stumpf et al 1998) uses this method to determine the center of a circulation. For the LLSD rotation, the center of circulation was considered to be at the LLSD rotation maximum.

The errors in range (Fig. 4) for both methods are quite similar, although the variance is smaller for the LLSD estimate. However, the azimuthal distance errors (Fig. 5) for the peak-to-peak method are significantly larger than the LLSD. Additionally, the distribution of the peak-to-peak location estimates is not Gaussian. This is illustrated in Fig. 6. While the LLSD position estimates are clustered around the center of the diagram, there are three distinct groupings for the peak-to-peak data. Because the peak-to-peak method only uses two data points in its

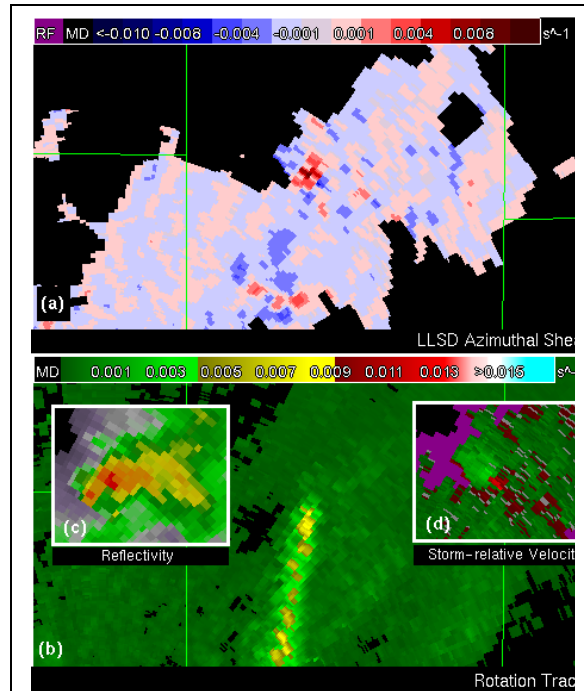


Figure 7: Insets (c) and (d) show conventional displays of reflectivity and velocity data available from Doppler weather radar. The image in (a) is a depiction of shear within the storm that is computed from the velocity data shown in (d). The red spots indicate locations with high shear. A slow northward movement of the high-shear areas with time is depicted as “rotation tracks” in (b). The graphic in (b) summarizes hours of velocity data into information a human decision maker can immediately use. (Scharfenberg et al. 2004).

calculations, it is highly susceptible to errors caused by the radial offset from the center of the circulation and noise.

4. LLSD Radial Divergence

LLSD radial divergence values are calculated for simulated divergence signatures of various sizes at different ranges from a hypothetical radar with 1° azimuthal spacing and 250 m range sampling. Results will be shown in the accompanying poster presentation.

5. Application

LLSD products have been successfully tested in an operation environment over a period of several convective seasons (Scharfenberg et

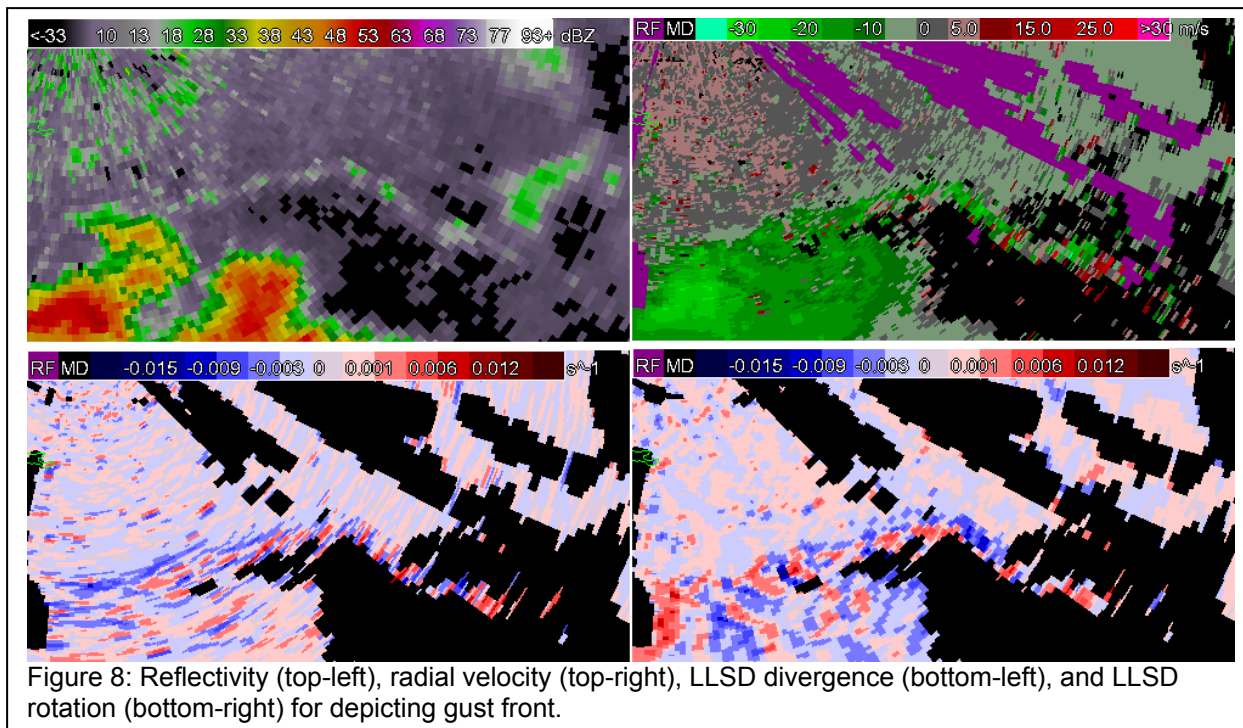


Figure 8: Reflectivity (top-left), radial velocity (top-right), LLSD divergence (bottom-left), and LLSD rotation (bottom-right) for depicting gust front.

al. 2004, Stumpf et al.). LLSD azimuthal shear may be used to locate areas of rotation within a storm cell and to assess the history of the circulation signature (Fig. 7). This, in turn, has been used to locate areas where damage assessments crews should focus their efforts during post-event damage surveys.

LLSD divergence and azimuthal shear fields may be combined to assess the presence of radar-detectable boundaries. Figure 8 shows a gust front, which is most notable in the divergence field in this example. Typically, boundaries that run perpendicular to the radar beam may be seen in the divergent LLSD field as convergence, while those parallel to the beam are better seen in the rotational LLSD field. Image processing applications may make use of these data to better identify boundary signatures.

6. Conclusion

The local, linear, least squares approach to calculating radial velocity derivatives is a vast improvement over the frequently-used but simplistic and grossly inaccurate method of calculating shear from two data points. The LLSD provides relatively smooth fields that may be used in other applications to identify features such as boundaries and vortices, as well as to accurately assess their strength and position.

7. Acknowledgements

Thanks to Amanda Adams for assisting with figures. Funding for this research was provided under NOAA-OU Cooperative Agreement NA17RJ1227, National Science Foundation Grants 9982299 and 0205628. This research is in response to requirements and funding by the Federal Aviation Administration (FAA). The views expressed are those of the authors and do not necessarily represent the official policy or position of the FAA.

8. References

Elmore, K.M, E.D. Albo, R.K. Goodrich, and D.J. Peters, 1994: NASA/NCAR airborne and ground-based wind shear studies. Final Report, contract no. NCC1-155, 343 pp.

Mitchell, E.D., and K.E. Elmore, 1998: A technique for identifying regions of high shear associated with mesocyclones and tornadic vortex signatures. Preprints, 14th Intl. Conf. on Interactive Information and Processing Systems for Meteor., Oceanography, and Hydrology, Phoenix, AZ, Amer. Met. Soc., 312-315.

Scharfenberg, K. A., D. J. Miller, D. L. Andra, Jr., and M. Foster, 2004: Overview of spring WDSS-II demonstration at WFO Norman. *22nd Conference on Severe Local Storms*, Hyannis, MA, Amer. Met. Soc. CD preprints.

Smith, T.M., K.E. Elmore, and S.A. Myers-Dulin, 2003: A Damaging Downburst Prediction and Detection Algorithm for the WSR-88D. *Wea. Forecasting* (in press).

Stumpf, G. J., T. M. Smith, K. L. Manross, and A. E. Gerard, 2003: Warning Decision Support System-Integrated Information (WDSS-II). Part II: Real-time test at Jackson Mississippi NWSFO. Preprints, 19th International Conference on Interactive Information Processing Systems for Meteorology, Oceanography, and Hydrology, Long Beach, CA, Amer. Met. Soc. - CD preprints.

Stumpf, G.J., A. Witt, E.D. Mitchell, P.L. Spencer, J.T. Johnson, M.D. Eilts, K.W. Thomas, and D.W. Burgess, 1998: The National Severe Storms Laboratory Mesocyclone Detection Algorithm for the WSR-88D. *Wea. Forecasting*, **13**, 304-326.

Wood, V. T., and R. A. Brown, 1997: Effects of radar sampling on single-Doppler velocity signatures of mesocyclones and tornadoes. *Wea. Forecasting*, **12**, 928-938.

Wood, V. T., and R. A. Brown, 2000: Oscillations in mesocyclone signatures with range owing to azimuthal radar sampling. *J. Atmos. Oceanic Tech.*, **17**, 90-95.